Article:
Do, H.-B. orcid.org/0000-0003-3274-5050, Le, D.-N., Nguyen, T.-H. et al. (7 more authors) (2024) Recycling of reduced graphene oxide from graphite rods in disposable zinc battery applicable to optical sensing. Ceramics International, 50 (21). pp. 43754-43762. ISSN 0272-8842

https://doi.org/10.1016/j.ceramint.2024.08.228

Recycling of reduced graphene oxide from graphite rods in disposable zinc battery applicable to optical sensing

Huy-Binh Do[a,*], Dong-Nghi Le[a], Tuan-Huu Nguyen[a], Van Toan Nguyen[b,c,*], Anh-Vu Phan-Gia[a], Ta Dinh Hien[a], Hoang-Minh Le[d], Phuong V. Pham[e,*], Maria Merlyne De Souza[f], Nam Nguyen Dang[b,c]

[a]Faculty of Applied Science, Ho Chi Minh City University of Technology and Education, Ho Chi Minh City 700000, Vietnam

[b]Future Materials & Devices Lab., Institute of Fundamental and Applied Sciences, Duy Tan University, Ho Chi Minh 700000, Vietnam

[c]The Faculty of Environmental and Chemical Engineering, Duy Tan University, Danang, 55000, Viet Nam

[d]Faculty of electrical and electronics engineering, Ho Chi Minh City University of Technology and Education, Ho Chi Minh City 700000, Vietnam

[e]Department of Physics, National Sun Yat-sen University, Kaohsiung 80424, Taiwan

[f]EEE Department, University of Sheffield, Sheffield S13JD, UK

Email addresses: binhdh@hcmute.edu.vn; phuongpham@mail.nsysu.edu.tw; nguyenvantoan8@duytan.edu.vn

ABSTRACT

We report a low cost, simple method to fabricate reduced graphene oxide (rGO) optical sensors from recycled batteries. The rGO nanosheets were exfoliated by electrochemical method under the assistant of electric arc using 5% KOH or NaOH electrolytes. The rGO nanosheets show interlayer distances ranging from 3.98 to 6.22 Å, and thicknesses from 0.62 to 6.00 nm, corresponding from 1 to 10 layers, respectively, determined from X-ray diffraction (XRD), atomic force microscopy (AFM), and transmission electron microscopy (TEM) measurements. Selected area electron diffraction (SAED) measurement indicates that rGO nanosheets content Miller-Bravais indices of (1-210) and (0-110) planes, and the hexagonal diffraction pattern of (0-110) plane of graphene sheets with d-spacing of 2.13 Å. Low defect densities in exfoliated rGO nanosheets were

confirmed by I_D/I_G ratios ~ 0.16 to 0.18 via Raman. The rGO nanosheets exfoliated in NaOH electrolyte have 19.35% lower oxygen content compared to those exfoliated in KOH electrolyte inspected from XPS spectra. The performance of the rGO optical sensors is controlled by defects created from oxygen functional groups formed during exfoliation process. The responsivity and response (rise) time of NaOH-exfoliated rGO sensor are 0.46 A/W and 2.3 s, respectively. These values are 21% (for responsivity) larger and 35% (for rise time) smaller than those of KOH-exfoliated rGO sensor. The best-in-class of high gain were demonstrated in this study for the rGO optical sensors prepared from disposed graphite rods. The results demonstrate how disposed batteries can be recycled to produce photodetectors and other optoelectronic devices using cheap and relatively nontoxic methods.

Keywords: Reduced graphene oxide; Electrochemical exfoliation; Electric arc; rGO optical sensors; Disposed batteries

1. Introduction

Graphene oxide (GO) has high potential in upcoming applications of electronic and optoelectronics devices [1-4] due to its tunable band gap from 0.11 to 3.0 eV [5]. Electrically insulating GO [6] can be converted to semi-conductive reduced graphene oxide (rGO) [7] using thermal, chemical, and photothermal reduction for applications in energy storage, electronic devices, biosensors, electrochemical sensors, and light sensors [8-16]. The concentration of oxygen functional groups can vary the bandgap of rGO from 1.1 to 1.9 eV [17]. The 2D delocalization of electrons in rGO results in an electron mobility greater than 300 $cm^2\ V^{-2}\ s^{-1}$ [18], much higher than typical organic semiconductors (< 1 $cm^2\ V^{-2}\ s^{-1}$) [19]. Hummer's methods are still the most widely used for GO synthesis due to its simplicity [20-22]. However, the strong oxidants such as $KMnO_4$, H_2SO_4, H_3PO_4, H_2O_2, and HCl, it requires are harmful to the environment [23]. Therefore, electrochemical methods have been explored as an alternative method to fabricate graphene and graphene oxide because its electrolytes are not as toxic [24, 25]. Electrochemical exfoliation also opens up opportunities to recycle disposed graphite rods from batteries that constitute an abundant cheap resource. It was reported that around 2.4 billion batteries are disposed in the United State every year alone [26]. Moreover, manufacturing rGO sensors from disposed graphite is a potential pathway towards a high value circular economy that generates products from waste.

Photodetectors have wide applications in various industry, however, current technology based on semiconductor-photodetectors has drawbacks such as high cost, complicated manufacturing, toxicity, low operating temperature, and scarcity [27]. The figure of merit of optical sensors is typically based on their response as a function of input power and their response time. Abid et al. fabricated optical sensors on rGO film prepared by vacuum filtration with a response of 1×10^{-4}

A/W in 1.5 s under the excitation of a 635 nm light source [10]. Using laser writing techniques, J. An and coauthors fabricated light sensors of rGO-ZnO composites. Their study recorded a high response of 3.24 A/W with a response time of 17.9 s under 365 nm light source excitation [28]. Quantum dots in WS_2 integrated on rGO coated on cotton textiles illustrated a response of 5.2×10^{-3} A/W under 1.57 s with a 405 nm illumination source [29]. Bonavolontà et al. fabricated rGO optical sensors on n-type Si substrate and obtained 0.2 A/W with a response time of 1.9 s under 685 nm illumination source [30]. Plasmonic nanoparticles have been confirmed to enhance the absorption of UV-VIS light [31], and its integration in rGO demonstrated a superior performance of optical sensors. Singh et al. attached plasmonic Au nanoparticles to GO and obtained extremely high response of 10 A/W with ultra-short time of 2.5×10^{-5} s under 405 nm illumination [32].

This work highlights the procedure to exfoliate rGO nanosheets in KOH or NaOH electrolyte using a specially designed electrochemical cell with electrodes that are able to move freely in the vertical direction as shown in Fig. 1. With the assistance of an electric arc in liquid, the rGO nanosheets were exfoliated directly on to the cathode (video, Supplementary 1). The rGO nanosheets were then utilized to fabricate rGO optical sensors.

2. Experimental details

Graphite rods collected from disposed Zn batteries shown in Fig. 1 underwent a cleaning process: (i) rinsing under water, (ii) grinding to sharpen the end as illustrated in Fig. S1, Supplementary 2. (iii) Rinsing graphite rods again under water, (iv) sonication in acetone, IPA and DI water. All rods were then rinsed in air at 80 ^{o}C for 24 hours. The rGO samples were exfoliated in 5% KOH (> 85%, Chemicals Duksan, South Korea) or 5% NaOH (>99%, Merck, Germany) electrolytes using the electrochemical setup in Fig. S2(a), Supplementary 2. Dilute 5% KOH and 5% NaOH are used due to their two advantages. First, dilute KOH and NaOH are cheaper and less toxic than

other strong oxidizing chemicals. Second, the products of the electrochemical reaction are H_2 and H_2O, relative safety to environment and human body. The cathode was connected to the graphite rod, while the anode was connected to stainless steel. The voltage was kept at 60.0 V during the experiment. Video of the exfoliation process is shown in Supplementary 1. The rGO solution in Fig. S2(b) was then filtered using vacuum filtration, followed by rinsing in air. The rGO powder was obtained in Fig. S2(c).

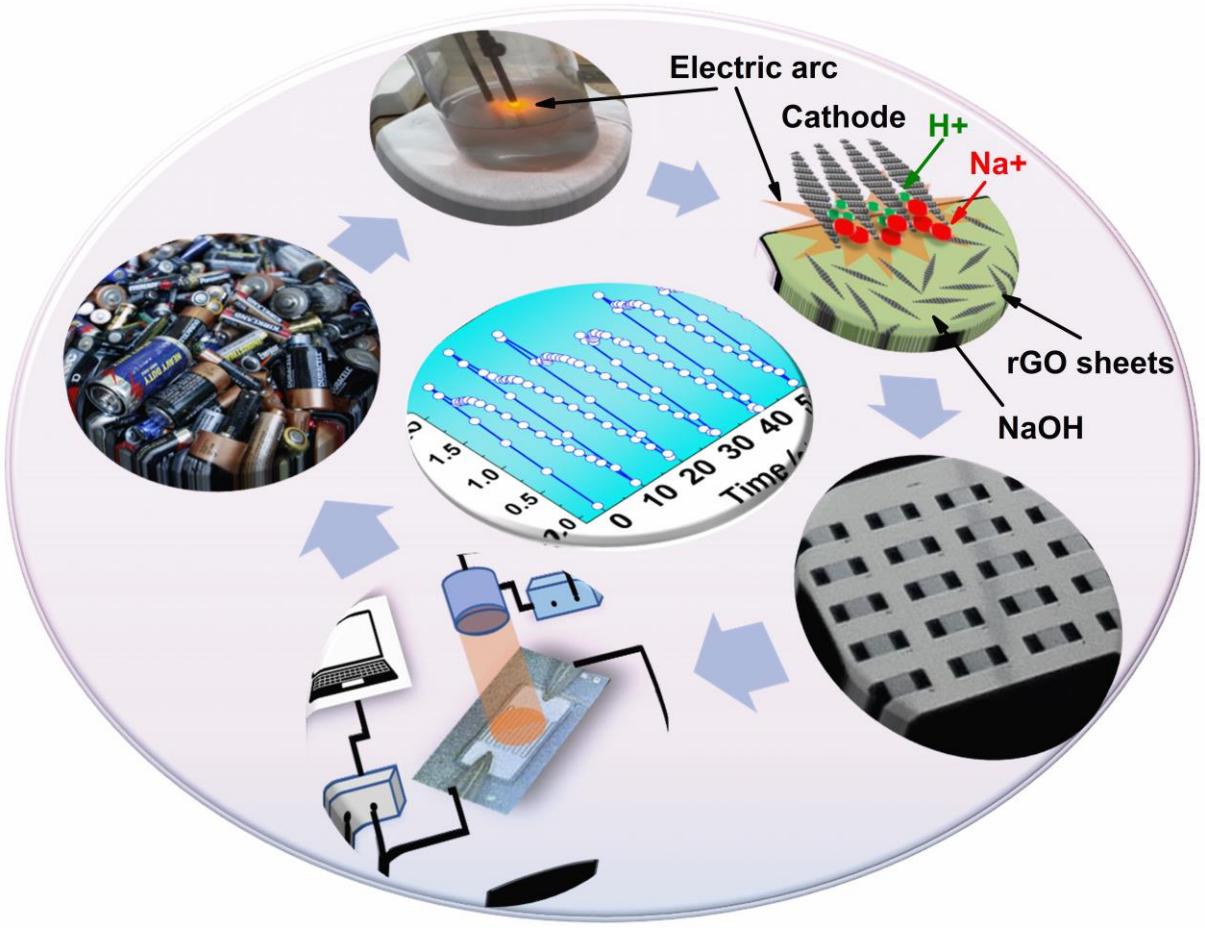

Figure 1. Schematic illustration of rGO recycling and rGO sensor fabrication.

The surface topography of rGO was examined via field emission scanning electron microscopy (FE-SEM), and its elemental composition determined by energy dispersive spectroscopy (EDS) (S-4800 FESEM Hitachi). Transmission electron microscopy (TEM) has the potential to clarify

the crystallinity as well as morphology of nanomaterials and has been extensively used to study rGO nanosheets (TEM: JEM-3010, JAPAN).

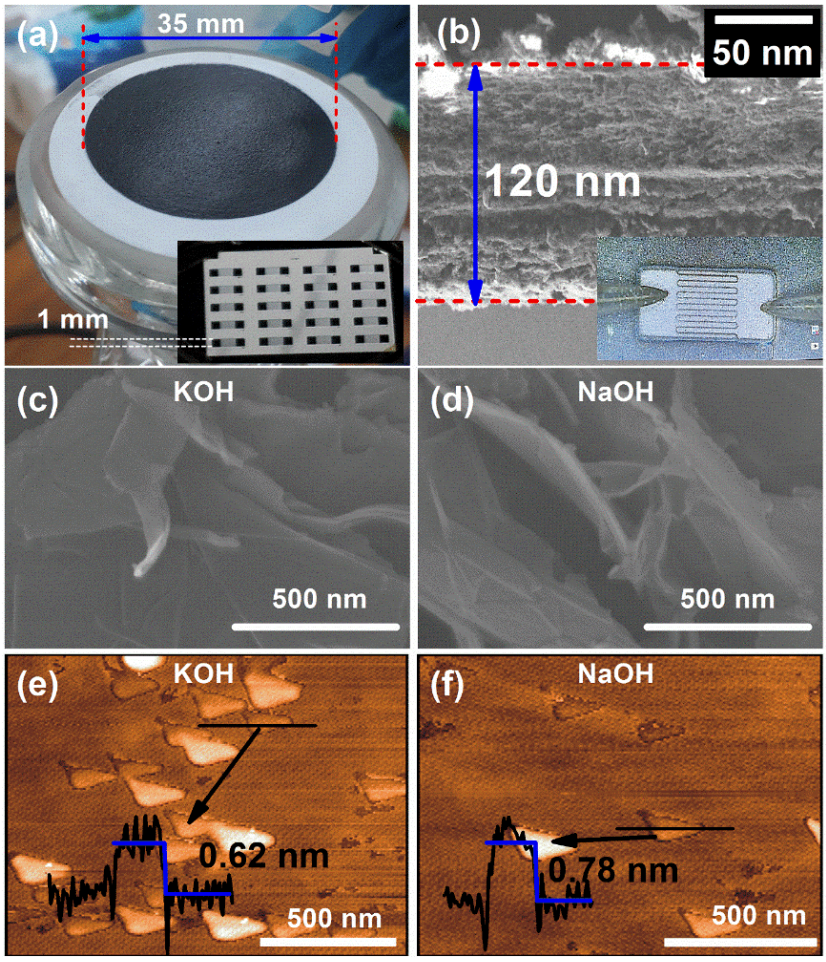

Figure 2. (a) rGO films prepared by vacuum filtration method, (b) SEM cross-section of rGO film deposited by vacuum filtration method. The film thickness is determined to be ~ 120 nm; Inset of (a) and (b) The shadow mask for fabrication of resistivity sensors, and the rGO resistivity sensor with Ti/W electrodes, respectively. (c) and (d) SEM images of rGO exfoliated in KOH and NaOH electrolytes, respectively, (e) and (f) AFM images and the thicknesses of rGO exfoliated in KOH and NaOH electrolytes, respectively.

The rGO film thickness was measured using atomic force microscopy (AFM) (MFP-3D AFM, US), and the chemical groups and defects in rGO samples were investigated via Fourier-transform

infrared spectroscopy (FTIR) (NICOLET 6700, Thermo) and Raman spectroscopy (XploRA PLUS, Horiba) with a 532 nm (2.33 eV) excitation source, respectively. The phase identification of rGO was analyzed using X-ray diffraction (XRD) (EMPYREAN, Panalytical), using K_α radiation (λ= 1.5406 Å). The XPS spectra were measured via JPS-9030 Photoelectron Spectrometer (JEOL) using K_α X-ray and analyzed by built-in software Specsurf 1.9.6. Charging effects were removed by considering C 1s at 284.8 eV and shifting the rest of the peaks accordingly.

The rGO sensor fabrication procedure is as follows: (i) deposit rGO film using vacuum filtration technique shown in Fig. 2(a). In this process, dry rGO powder is distilled in DI water at a concentration of 3 mg rGO/1 ml DI, then 5 ml rGO solution is dropped on the acetate cellulose filter (pore size of 0.22 µm) under vacuum to form rGO membranes with a thickness of ~ 120 nm determined from SEM cross-section measurement shown in Fig. 2(b). (ii) The electrodes of sensors are formed using a shadow mask shown in the inset of Fig. 2(a) with the electrode distance of 50 µm. The samples are then loaded into a sputtering chamber to deposit Ti/W (~ 30 nm/200 nm). Ti and W metals are chosen because they are cheap as compared with Au. The electron affinity of rGO was reported at 3.4 eV [32], so Ti layer (with the work function of 4.3 eV) lowers the Schottky barrier of Ti/rGO interface. Besides the low price, W is used as a capping layer to protect Ti layer from damaging and oxidizing. The I-V and I-t characteristics are measured using the Ossila Source Measure Unit P2005A2 (Ossila, UK). The excitation light sources are a violet laser with λ = 405 nm and a red laser with λ = 650 nm.

3. Results and discussion

Figure 2(c and d) shows the SEM images of rGO, illustrating the stacking of rGO nanosheets with some overlaps and wrinkles. Their AFM measurement in Fig. 2(e and f) indicates thickness

ranging from 0.62 to 6.00 nm, corresponding to one to ten layers with an average diameter of ~ 200 nm.

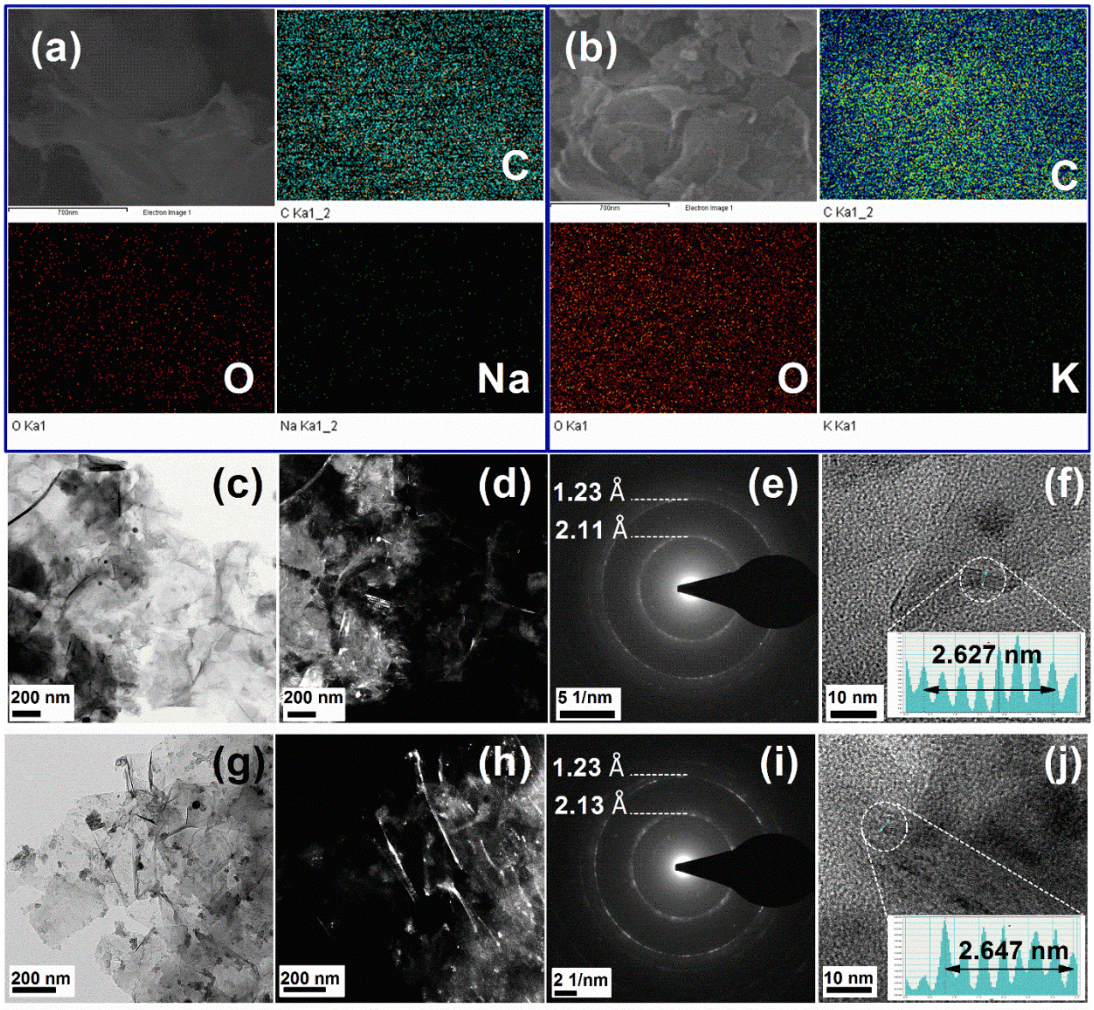

Figure 3. (a) and (b) EDS mapping of the composition of samples exfoliated in NaOH and KOH, respectively. (c) – (f) Bright field TEM image, dark field TEM image, SEAD pattern, and the high-resolution TEM image of KOH exfoliated sample, respectively. (g) – (j) Bright field TEM image, dark field TEM image, SEAD pattern, and the high-resolution TEM image of NaOH exfoliated sample, respectively. Inset of Figs. 3(f) and (j) show the crystalline space analysis of the positions marked on the same figures.

EDS mapping shown in Fig. 3(a and b) illustrates the presence of K and Na atoms on the exfoliated rGO, indicating that K and Na atoms are still attached onto the rGO sheets after they intercalate into the graphite and the exfoliated graphite rod to form the rGO layers. The C concentration in NaOH exfoliated sample is significantly higher than that in the KOH sample, and the opposite is also observed for O concentration. Fig. 3(a and b) shows an even distribution of K and Na atoms without any agglomeration on rGO nanosheets. The alkaline doping using other methods showed a tendency to form alkaline particles on graphene sheets because of the lack of active sites to interact with these atoms [33].

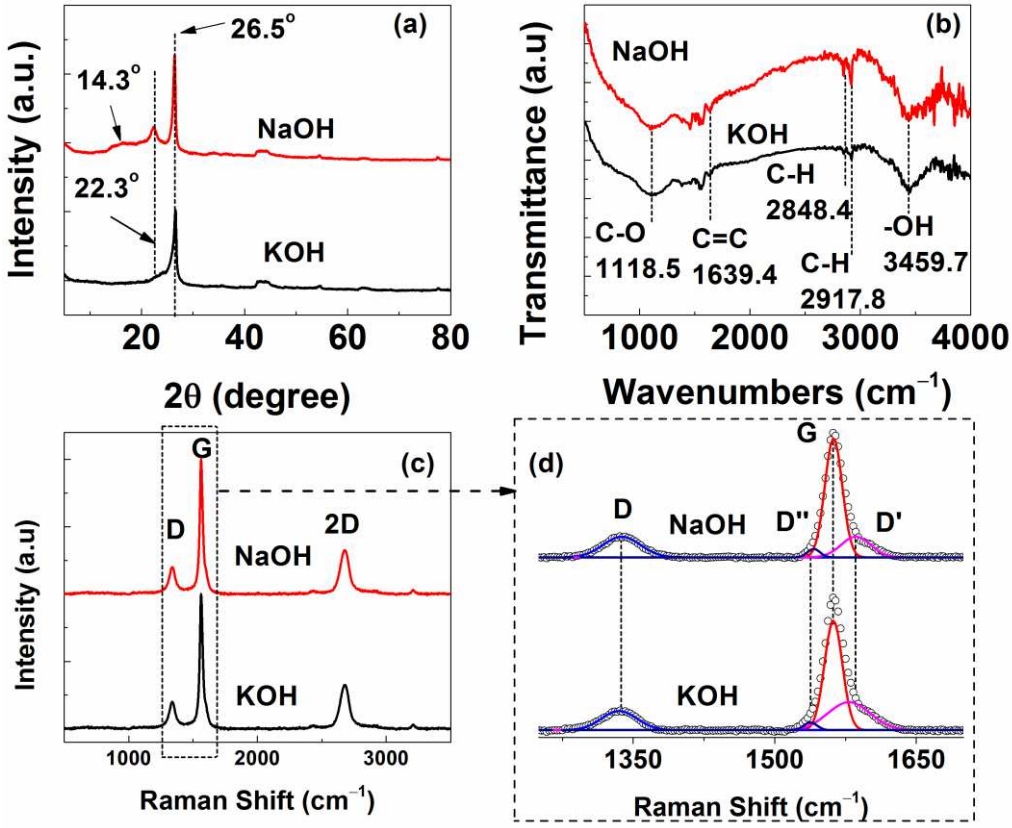

Figure 4. (a) XRD, (b) FTIR, and (c) Raman spectra of rGO exfoliated in KOH and NaOH electrolytes from disposed graphite rods. (d) The decomposition of D and G Raman peaks shown in Fig. 4(c).

The TEM images and profile analysis of rGO nanosheets are shown in Fig. 3(c - j). The bright field and dark field TEM images of both samples shown in Fig. 3(c and d), and Fig. 3(g and h) indicate that the rGO nanosheets have mixed structures of single as well as multilayers. The SEAD images shown in Fig. 3(e and i) reveal the same diffraction rings at 1.23 and 2.13 Å, corresponding to Miller-Bravais indices of (1-210) and (0-110) planes, respectively [34]. The spacing of 2.13 Å in both samples confirm the hexagonal diffraction pattern of (0-110) plane of graphene sheets. High resolution TEM images shown in Fig. 3(f and j) combined with the crystalline space analysis of the position within 8 layers indicate that the d-spacing between 2 layers of graphene is 3.75 Å.

The crystal structure of rGO samples is verified in Fig. 4(a). A strong and sharp diffraction peak is observed at 26.5°, corresponding to the small interlayer distances (3.37 Å) of multilayer rGO nanosheets and graphite. The emergence of peaks at 14.3 and 22.3° in KOH and NaOH samples indicates that oxygen functional- and epoxy groups are introduced in between consecutive layers. The interlayer distances are correspondingly 6.22 Å (2θ = 14.3°) and 3.98 Å (2θ = 22.3°), respectively. The chemical groups in rGO samples were identified in Fig. 4(b). The main peak centers are located at 1118.5, 1639.4, 2848.4, 2917.8, and 3459.7 cm^{-1}, which can be related to C-O, C=C , C-H (2848.4, 2917.8 cm^{-1}), and -OH stretching respectively [35]. The Raman spectra of the same samples and the devolution of their G peaks are shown in Fig. 4(c and d), respectively. It is seen that the edge deformation in rGO nanosheets exfoliated in KOH and NaOH electrolytes is less than that in GO fabricated by Hummer's method [10], illustrated by the fact that the I_D/I_G ratios of NaOH-rGO sample and KOH-rGO sample are 0.16 and 0.18, respectively. Fig. 4(d) shows the devolution of D and G peaks illustrated in Fig. 4(c). The G peak (1562.9 cm^{-1}) is from the in-plane vibrations of sp^2 carbon atoms. The amount of disorder in rGO nanosheets is deconvoluted into two separate disorder peaks: D (1338.7 cm^{-1}) from the intervalley scattering,

and D' (1587.2 cm^{-1}), from intravalley scattering for both samples [36, 37]. The fact that the intensity of D' band of KOH sample is 26.7% higher than that of NaOH sample indicates that less defects can be obtained in rGO prepared in NaOH electrolyte. The results are in agreement with those in SEAD measurement shown in Fig. 3(e and i). Small intensity of D" band was observed in both samples because of the presence of a small amount of amorphous carbon in the disposed graphite rode [36].

Table 1. Core peaks of C 1s, K 2p, and Na 1s of KOH and NaOH after the deconvolution. The unit is eV.

Peaks		KOH sample	NaOH sample	references
C 1s	C-C, C-H	284.8	284.8	[38]
	C-O	286.7	286.3	[39]
	C=O	287.7	287.9	[39]
	O-C=O	289.0	292.7	[39]
	C-Na		282.9	[40]
	C-K	282.8	-	[40]
K 2p 3/2	K 2p 3/2	295.0	-	[41]
	K 2p 1/2	297.8	-	[41]
Na 1s	Na-O	-	1071.7	[42]
	Na-C	-	1074.2	[43]

Figure 5(a) shows wide-scan X-ray photoelectron spectroscopy (XPS) spectra of rGO nanosheets exfoliated in both KOH and NaOH. Both samples were dispersed in water, followed by sonication and coated on SiO_2/Si substrate before they were loaded into the XPS chamber. All peaks are calibrated by placing the C 1s peak at a binding energy of 284.8 eV and shifting the rest

of the peaks accordingly. The shift of peaks in XPS measurement is due to sample charging effects. For wide-scan XPS spectra, the strongest peak is C 1s at 284.8 eV in both samples, and the O 1s peaks is determined at 532.9 eV, which can be due to the overlap of aliphatic C-OH peak (532.9 eV), aromatic C-OH peak (533.6 eV), and Si-O peak (532.62 eV)[38]. The atomic percent of the NaOH sample is 75.53% C, 14.72% O and 9.75% Na, calculated based on the intensity of C 1s, O 1s, Na 1s peaks in the wide-scan spectra shown in Fig. 5(a). The atomic percent is determined to decrease to 59.27% for C, increase to 34.07% for O, and be 6.66% for K in KOH sample. The present of Na and K peaks in the wide-scan XPS spectra indicate that these alkaline metal elements were absorbed on rGO nanosheets.

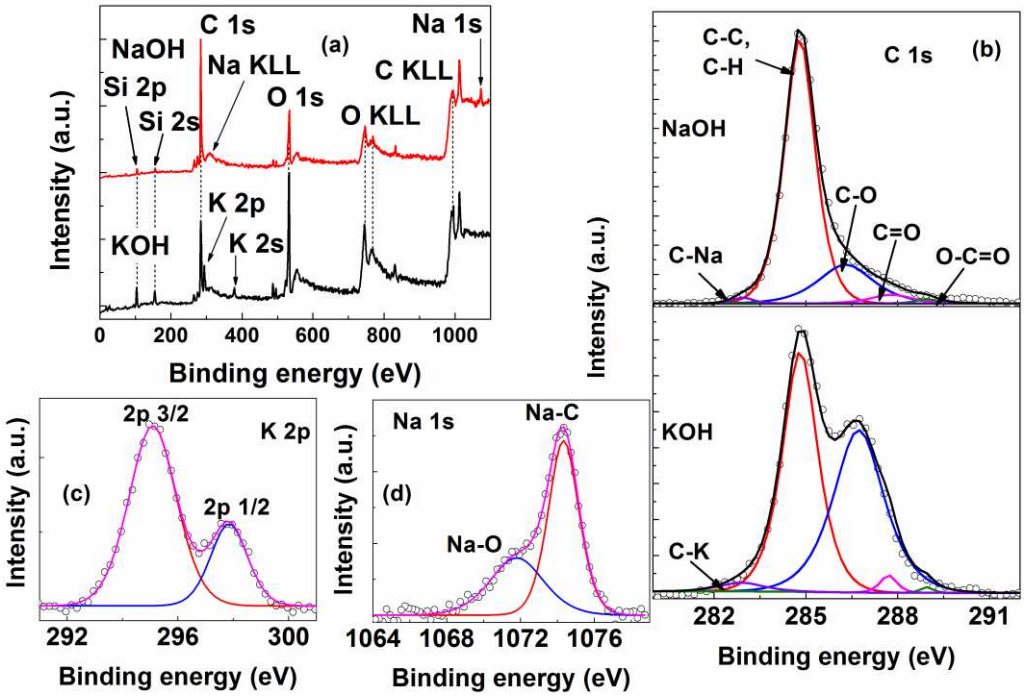

Figure 5. XPS spectra of rGO exfoliated in KOH and NaOH electrolytes. (a) Survey scan, (b) high resolution spectra of C 1s of KOH and NaOH samples, (c) K 2p of KOH sample, and (d) Na 1s of NaOH sample.

The atomic percentage of oxygen in NaOH sample is lower than that in the KOH sample suggesting that number of oxygen functional groups replaced by Na atoms are more than those

replaced by K atoms, referring to an effectively partial reduction of GO layers during the exfoliation process in NaOH electrolyte. Alkaline dopants were reported to increase the conductivity by 10 times as compared to undoped GO [44]. The results are in agreement with the EDS mapping shown in Fig. 3(a and b). The core level of C 1s, K 2p, and Na 1s peaks were deconvoluted as shown in Fig. 5(b - d) and Table 1, using Gaussian–Lorentz line shape and a Shirley background with an uncertainty of the core position of 0.05 eV. C 1s peaks are deconvoluted to 5 peaks, including C-C, C-H, C-O, C=O, O-C=O peaks [39, 40]. The increase in magnitude of the C-O peak in the KOH sample indicates that the exfoliation strongly oxidizes graphene sheets via the C-O bond. A small binding energy at 282.9 and 282.8 eV shown in Fig. 5(b) can be assigned to the C-Na bond in the NaOH sample and the C-K bond in the KOH sample, respectively [40], indicating that alkaline atoms were doped on rGO nanosheets effectively. Because the K 2p peak is clearly separated to C 1s peak in the wide-scan XPS spectra and the observation of K 2s peak, the deconvolution of K 2p peak is conducted in Fig. 5(c), with a binding energy at 295.0 eV, and 297.8 eV for K 2p3/2 and K 2p1/2, respectively. Na 1s peak is deconvoluted in Fig. 5(d), showing a specific Na-O bond at 1071.7 eV [42]. New and strong peak observed at 1074.2 eV is due to the absorption of Na on graphene sheets, denoted Na-C bond [43]. The 1.2 eV shift of the Na 1s peak was also observed in another study when Na was absorbed on the C-ring of tetracyanoquinodimethane[43]. The present of K 2p, C-K bonds, Na 1s and C-Na bonds confirms the intercalation of K and Na atoms into graphite during the electrochemical exfoliation assisted by an electric arc.

Figure 6(a-d) shows the current – time characteristics of resistive optical sensors fabricated from rGO nanosheets exfoliated in KOH and NaOH electrolytes. Their photoresponse in terms of change in current is measured at a constant intensity of incident light having the wavelengths of

405 and 650 nm. The wavelengths of 405 nm and 650 nm are chosen to understand the effects of oxygen functional groups on the band gap of rGO because its band gap may vary from 1.9 eV (652.5 nm) to 3.0 eV (413.3 nm) [5, 17]. The sensor stability and repeatability in response to the photocurrent is calculated using the formula:

$$I_{ph} = I_{light} - I_{dark} \quad (1)$$

where I_{ph} is photocurrent, I_{light} is light current, and I_{dark} is dark current.

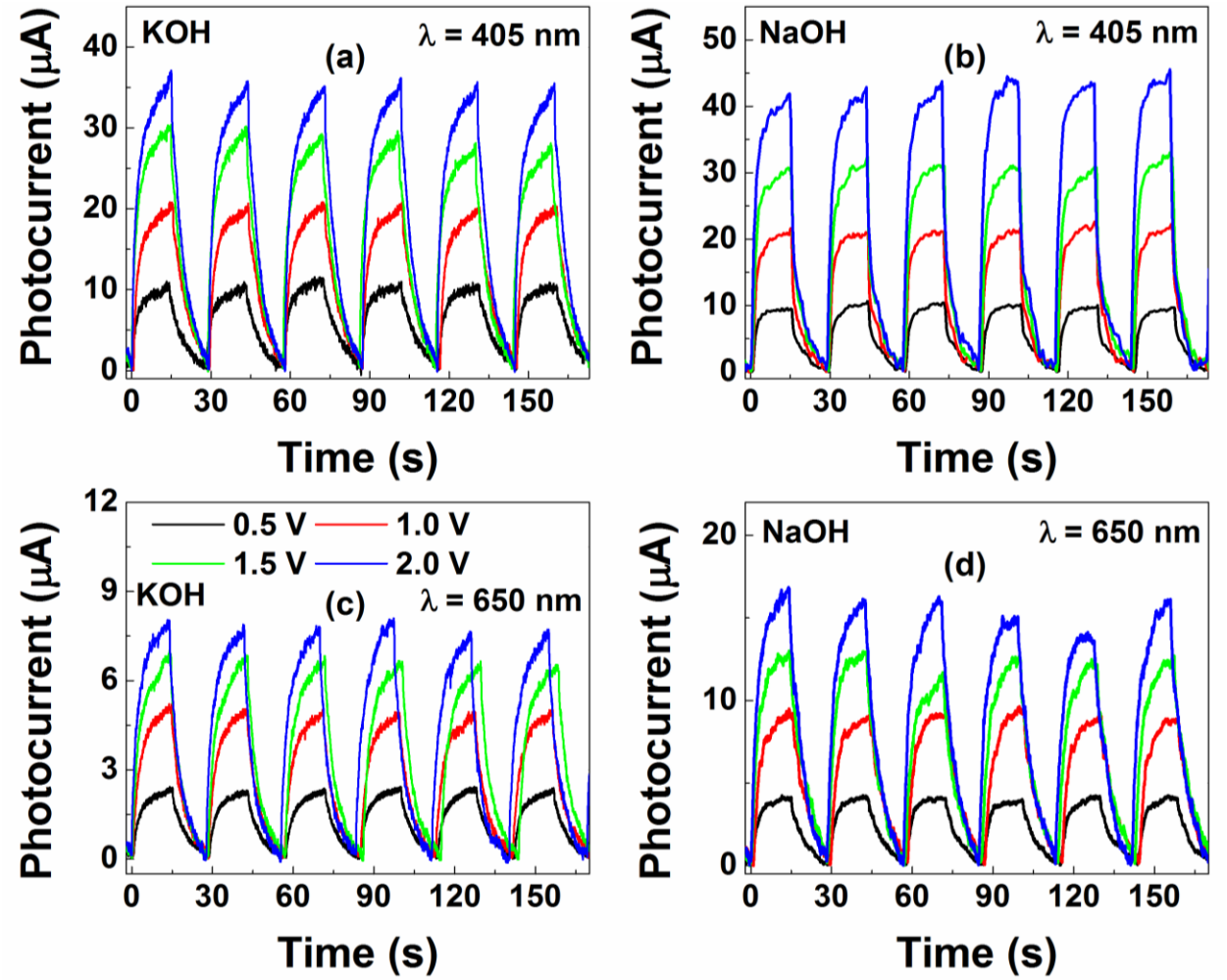

Figure 6. (a – d) Current – time characteristics for several cycles as light is turned on and off with the excited wavelength of 405 nm and 650 nm, the voltage applied between two electrodes are 0.5 – 2.0 V, and the power of the light is 45 mW/cm^2.

The values of I_{ph} as a function of time and wavelength are illustrated in Fig. 7(a), showing that at bias voltages ranging from 0.5 to 2.0 V, I_{ph} significantly increases at excited wavelength of 405 nm, and gradually increases at that of 650 nm. The lower currents at excited light source of 650 nm resulted from photons with insufficient energy, only generating free photo-generated charges in rGO films having the band gap $E_g \leq 1.91$ eV. In contrast, 405 nm laser (photon energy E_v of 3.07 eV) can excite electrons in all rGO films that have the band gap ranging from 0.11 to 3.0 eV [17]. To investigate the performance of rGO sensors, photocurrent, response time (rise and fall), and responsivity are investigated in Fig. 7(b – e), respectively. High photocurrents of 43.43 μA for NaOH-exfoliated sensor and 36.18 μA for KOH-exfoliated one are obtained at voltage of 2.0 V and excited wavelength of 405 nm shown in Fig. 7(b). The linear relationship of I_{ph} – V curves is observed in both devices at $\lambda = 405$ nm. The slope of the NaOH-exfoliated sensor is higher than that of the KOH-exfoliated one, indicating low sheet resistivity of rGO film fabricated from NaOH-exfoliated rGO nanosheets. The results are confirmed by the low densities of defects in rGO nanosheets which are believed to be due to oxygen functional groups, investigated in Fig. 4 (d) and Fig. 5 (b). These defects can trap the photo-generated carriers in rGO film. The current in this case should be from swift transportation of the photo-generated charges from rGO to metal electrodes. At $\lambda = 650$ nm, the non-linear I-V curves are observed in bias voltages ranging from 1.0 to 2.0 V in both sensors shown in Fig. 7(b), namely the saturation regions of photocurrents observed in the previous study [32]. The saturation current of NaOH-exfoliated rGO sensor is 81.5% higher than that of KOH-exfoliated rGO one, probably due to the low defect density of NaOH-exfoliated rGO nanosheets.

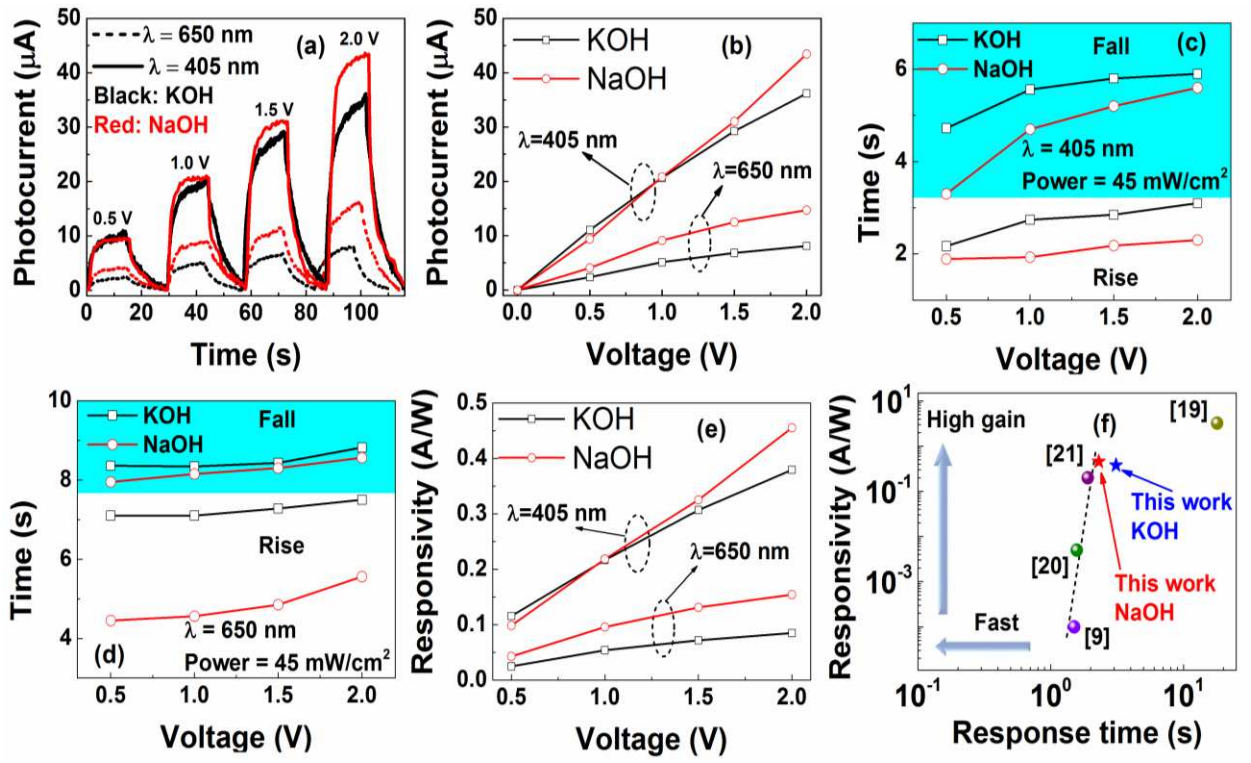

Figure 7. (a) Comparison of the temporal photocurrent response of KOH- and NaOH-exfoliated sensors at bias voltages ranging from 0.5 V to 2.0 V, (b) I_{ph} – V characteristics of KOH- and NaOH-exfoliated sensors at excited wavelengths of 405 nm and 650 nm, (c) and (d) Rise time and fall time of KOH- and NaOH-exfoliated sensors as a function of bias voltages, excited by the wavelengths of 405 nm and 650 nm, respectively, (e) Responsivity – voltage curves of KOH- and NaOH-exfoliated sensors excited by the wavelengths of 405 and 650 nm, and (f) Benchmarking of responsivity versus rise time of rGO and GO photosensors. The dash line is used to compare the results in this study to those in literatures.

It was suggested that the photoconductive effect is the dominant mechanism of photocurrent generation in rGO-based photodetectors [45]. The general process should be (i) generation of carriers by absorption of the incident light, (ii) transport of carriers and (iii) extraction of carriers via the external circuit. All of these factors impact the response time and the photocurrent of the photodetectors. The rise time (t_1) is calculated from 10 to 90% amplitude of the dark current, and

recovery (fall) time (t_2) is from 90 to 10% amplitude of light current shown in Fig. 7(c) for λ = 405 nm, and Fig. (d) for λ = 650 nm. At λ = 405 nm, the rise times of NaOH-exfoliated rGO sensor are from 1.89 s (at 0.5 V) to 2.31 s (at 2.0 V), about 30% smaller than those of KOH-exfoliated rGO one shown in Fig. 7(c). The fall times are from 3.31 to 5.60 s for sensors exfoliated in NaOH electrolyte and from 4.73 to 5.92 s for ones exfoliated in KOH electrolyte. It is clear that rise time and fall time increase ~ 2 – 3 times when the excited wavelength increases from 405 to 650 nm, observed in both sensors shown in Fig. 7(d). The fact that the rise time of NaOH-exfoliated rGO sensor is smaller than that of KOH-exfoliated rGO sensor may originate from structure defects, which can capture the photo-generated carriers, as discussed in Raman spectra shown in Fig. 4(d) and XPS spectra shown in Fig. 5.

Fig. 7(e) shows the responsivity of NaOH- and KOH-exfoliated sensors, which is calculated from [32]:

$$R = \frac{J_{ph}}{P} \tag{2}$$

where J_{ph} and P are the photocurrent density and the power of the incident light, respectively. The responsivity of 0.46 A W^{-1} of NaOH-exfoliated rGO sensors (at V = 2.0 V and λ = 405 nm) is 17.4% higher than that of KOH-exfoliated rGO ones. These results are compared with those in the previous studies shown in the benchmark in Fig. 7(f) with an observed deviation of 4 orders of magnitude. The highest response (10 A/W) is from reference [32] because the plasmonic gold nanoparticles enhance light adsorption in the visible region. The devices fabricated in this study have highest performance as compared to others that do not use expensive materials [10, 28-30]. Figure 7(f) indicates that the optical sensors fabricated from NaOH-exfoliated nanosheets are the best-in-class in terms of response time and sensitivity.

4. Conclusion

An inexpensive price, convenient recycling method to manufacture rGO from graphite rods of Disposable Zinc batteries was successfully researched. The rGO samples prepared by electrochemical method under the assistant of electric arc showed superior properties of low defect density, illustrated by low I_D/I_G at 0.16 – 0.18, exfoliated in KOH and NaOH solutions. The rGO nanosheets have a thickness of 0.62 to 6.00 nm, corresponding to one to ten layers, determined from AFM and TEM measurements. The hexagonal diffraction pattern of (0-110) plane of graphene sheets in response to d-spacing of 2.13 Å was observed in both samples from SEAD measurement. XPS spectra illustrated that the oxidation of rGO exfoliated in NaOH electrolyte is 19.35% less than that exfoliated in KOH electrolyte, strongly affecting the response of the rGO optical devices. The sensitivity, response time, and recovery time were determined as 0.38 A/W, 3.1 s, and 5.9 s, respectively for KOH-exfoliated rGO sensor. These values were 0.46 A/W, 2.3 s, 5.6 s, respectively for NaOH-exfoliated rGO one. The best-in-class of high gain were demonstrated in this study for the rGO optical sensors prepared from disposed graphite rods.

Conflict of Interest - The authors declare no conflict of interest

Acknowledge - This work was funded by the Ho Chi Minh City University of Technology and Education, Vietnam (grant No. T2023-82).

References

[1] J. Wu, H. Lin, D.J. Moss, K.P. Loh, B. Jia, Graphene oxide for photonics, electronics and optoelectronics, Nat. Rev. Chem., 7 (2023) 162-183. https://doi.org/10.1038/s41570-022-00458-7

[2] P.V. Pham, T.-H. Mai, H.-B. Do, V.K. Ponnusamy, F.-C. Chuang, Integrated Graphene Heterostructures in Optical Sensing, Micromachines, 14 (2023) 1060. https://doi.org/10.3390/mi14051060

[3] M.A. Iqbal, M. Malik, T.K. Le, N. Anwar, S. Bakhsh, W. Shahid, S. Shahid, S. Irfan, M. Al-Bahrani, K. Morsy, H.-B. Do, V.K. Ponnusamy, P.V. Pham, Technological Evolution of Image Sensing Designed by Nanostructured Materials, ACS Mater. Lett., 5 (2023) 1027-1060. https://doi.org/10.1021/acsmaterialslett.2c01011

[4] Z. Ismail, Green reduction of graphene oxide by plant extracts: A short review, Ceram. Int., 45 (2019) 23857-23868. https://doi.org/10.1016/j.ceramint.2019.08.114

[5] H. Huang, Z. Li, J. She, W. Wang, Oxygen density dependent band gap of reduced graphene oxide, J. Appl. Phys., 111 (2012). https://doi.org/10.1063/1.3694665

[6] A. Nourbakhsh, M. Cantoro, T. Vosch, G. Pourtois, F. Clemente, M.H. van der Veen, J. Hofkens, M.M. Heyns, S. De Gendt, B.F. Sels, Bandgap opening in oxygen plasma-treated graphene, Nanotechnology, 21 (2010) 435203. https://doi.org/10.1088/0957-4484/21/43/435203

[7] R. Kazemzadeh, K. Andersen, L. Motha, W.S. Kim, Highly Sensitive Pressure Sensor Array With Photothermally Reduced Graphene Oxide, IEDL, 36 (2015) 180-182. https://doi.org/10.1109/led.2014.2385701

[8] Z. Bo, X. Shuai, S. Mao, H. Yang, J. Qian, J. Chen, J. Yan, K. Cen, Green preparation of reduced graphene oxide for sensing and energy storage applications, Sci. Rep., 4 (2014) 4684. https://doi.org/10.1038/srep04684

[9] D. Kadadou, L. Tizani, V.S. Wadi, F. Banat, V. Naddeo, H. Alsafar, A.F. Yousef, S.W. Hasan, Optimization of an rGO-based biosensor for the sensitive detection of bovine serum albumin: Effect of electric field on detection capability, Chemosphere, 301 (2022) 134700. https://doi.org/10.1016/j.chemosphere.2022.134700

[10] Abid, P. Sehrawat, S.S. Islam, P. Mishra, S. Ahmad, Reduced graphene oxide (rGO) based wideband optical sensor and the role of Temperature, Defect States and Quantum Efficiency, Sci. Rep., 8 (2018) 3537. https://doi.org/10.1038/s41598-018-21686-2

[11] P.V. Pham, T.-H. Mai, H.-B. Do, M. Vasundhara, V.-H. Nguyen, T. Nguyen, H.V. Bui, V.-D. Dao, R.K. Gupta, V.K. Ponnusamy, J.-H. Park, Layer-by-layer thinning of two-dimensional materials, Chem. Soc. Rev., 53 (2024) 5190-5226. https://doi.org/10.1039/d3cs00817g

[12] Rashi, Exploring the methods of synthesis, functionalization, and characterization of graphene and graphene oxide for supercapacitor applications, Ceram. Int., 49 (2023) 40-47. https://doi.org/10.1016/j.ceramint.2022.10.333

[13] T.P. Manh, N. Nguyen Van, V.B.T. Phung, L. Ngo Thi, Q. Ngo Quy, S. Le The, P. Doan Tien, D. Tran Quang, T. Nguyen Van, N. To Van, One-step preparation of Ni–Co binary metal sulfides on reduced graphene oxide for all-solid-state supercapacitor devices with enhanced electrochemical performance, Ceram. Int., 50 (2024) 22757-22770. https://doi.org/10.1016/j.ceramint.2024.03.378

[14] L.-H. Tseng, W.-C. Li, T.-C. Wen, The effectiveness of graphene oxide added in activated carbon for superior supercapacitor performance, J. Taiwan Inst. Chem. Eng., 143 (2023) 104684. https://doi.org/10.1016/j.jtice.2023.104684

[15] R.S. Uysal, A promising electrochemical sensor based on gold deposited-reduced graphene oxide sheets for the detection of Cd(II) and Pb(II), Chem. Pap., 78 (2024) 3589-3606. https://doi.org/10.1007/s11696-024-03330-8
[16] T.T.H. Nguyen, T.H.Y. Pham, T.D. Doan, N.H. Thi, H.T. Oanh, T.T. Nguyen, V.T.T. Ha, T. Van Nguyen, M.J. Cho, D.H. Choi, M.H. Hoang, Silver nanowire/graphene oxide electrode for electrochemical detection of lead ions, Chem. Pap., 76 (2022) 5459-5469. https://doi.org/10.1007/s11696-022-02254-5
[17] B. Ezhilmaran, A. Patra, S. Benny, S. M. R, A. V. V, S.V. Bhat, C.S. Rout, Recent developments in the photodetector applications of Schottky diodes based on 2D materials, J. Mater. Chem. C, 9 (2021) 6122-6150. https://doi.org/10.1039/d1tc00949d
[18] Y. Wang, Y. Chen, S.D. Lacey, L. Xu, H. Xie, T. Li, V.A. Danner, L. Hu, Reduced graphene oxide film with record-high conductivity and mobility, Mater. Today, 21 (2018) 186-192. https://doi.org/10.1016/j.mattod.2017.10.008
[19] V. Coropceanu, J. Cornil, D.A. da Silva Filho, Y. Olivier, R. Silbey, J.-L. Brédas, Charge Transport in Organic Semiconductors, Chem. Rev., 107 (2007) 926-952. https://doi.org/10.1021/cr050140x
[20] M.R. Karim, M.N. Uddin, M.A. Shaikh, M.S. Rahaman, I.A. Siddiquey, M.A. Arafath, M.S. Islam, S. Hayami, K.A. Alamry, A.M. Asiri, M.M. Rahman, Engineering tunable conductivity, p-n junction and light-harvesting semi-conductivity of graphene oxide by fixing reduction mood only, J. Taiwan Inst. Chem. Eng., 120 (2021) 325-335. https://doi.org/10.1016/j.jtice.2021.03.019
[21] C.-C. Fu, R.-S. Juang, M.M. Huq, C.-T. Hsieh, Enhanced adsorption and photodegradation of phenol in aqueous suspensions of titania/graphene oxide composite catalysts, J. Taiwan Inst. Chem. Eng., 67 (2016) 338-345. https://doi.org/10.1016/j.jtice.2016.07.043
[22] H. Korucu, A.I. Mohamed, A. Yartaşı, M. Uğur, The detailed Characterization of graphene oxide, Chem. Pap., 77 (2023) 5787-5806. https://doi.org/10.1007/s11696-023-02897-y
[23] A. Alkhouzaam, H. Qiblawey, M. Khraisheh, M. Atieh, M. Al-Ghouti, Synthesis of graphene oxides particle of high oxidation degree using a modified Hummers method, Ceram. Int., 46 (2020) 23997-24007. https://doi.org/10.1016/j.ceramint.2020.06.177
[24] T.Q. Toan, N.Q. Dung, M.X. Truong, P. Van Hao, T.N. Hien, N. Van Dang, L.P. Anh, N.X. Hoa, P.T. Thuy, D. Van Thanh, A nonenzymatic uric acid sensor based on electrophoretically deposited Graphene/ITO electrode, Vietnam J. Chem., 60 (2022) 60-65. https://doi.org/10.1002/vjch.202200071
[25] F. Liu, C. Wang, X. Sui, M.A. Riaz, M. Xu, L. Wei, Y. Chen, Synthesis of graphene materials by electrochemical exfoliation: Recent progress and future potential, Carbon Energy, 1 (2019) 173-199. https://doi.org/10.1002/cey2.14
[26] Sunaina, M. Sreekanth, M. Manolata Devi, V. Sethi, S. Ghosh, S.K. Mehta, A.K. Ganguli, M. Jha, New approach for fabrication of vertically oriented ZnO based field emitter derived from waste primary batteries, Mater. Sci. Eng. B, 274 (2021) 115480. https://doi.org/10.1016/j.mseb.2021.115480
[27] G. Li, L. Liu, G. Wu, W. Chen, S. Qin, Y. Wang, T. Zhang, Self-Powered UV–Near Infrared Photodetector Based on Reduced Graphene Oxide/n-Si Vertical Heterojunction, Small, 12 (2016) 5019-5026. https://doi.org/10.1002/smll.201600835
[28] J. An, T.-S.D. Le, C.H.J. Lim, V.T. Tran, Z. Zhan, Y. Gao, L. Zheng, G. Sun, Y.-J. Kim, Single-Step Selective Laser Writing of Flexible Photodetectors for Wearable Optoelectronics, Adv. Sci., 5 (2018) 1800496. https://doi.org/10.1002/advs.201800496

[29] Abid, P. Sehrawat, C.M. Julien, S.S. Islam, WS2 Quantum Dots on e-Textile as a Wearable UV Photodetector: How Well Reduced Graphene Oxide Can Serve as a Carrier Transport Medium?, ACS Appl. Mater. Interfaces, 12 (2020) 39730-39744. https://doi.org/10.1021/acsami.0c08028
[30] C. Bonavolontà, A. Vettoliere, G. Falco, C. Aramo, I. Rendina, B. Ruggiero, P. Silvestrini, M. Valentino, Reduced graphene oxide on silicon-based structure as novel broadband photodetector, Sci. Rep., 11 (2021) 13015. https://doi.org/10.1038/s41598-021-92518-z
[31] A. Amirjani, N.B. Amlashi, Z.S. Ahmadiani, Plasmon-Enhanced Photocatalysis Based on Plasmonic Nanoparticles for Energy and Environmental Solutions: A Review, ACS Appl. Nano Mater., 6 (2023) 9085-9123. https://doi.org/10.1021/acsanm.3c01671
[32] N.S. Singh, A.K. Mia, P. Giri, Role of oxygen functional groups and attachment of Au nanoparticles on graphene oxide sheets for improved photodetection performance, Nanoscale Adv., 6 (2024) 2136-2148. https://doi.org/10.1039/D3NA01120H
[33] K.C. Kwon, K.S. Choi, B.J. Kim, J.-L. Lee, S.Y. Kim, Work-Function Decrease of Graphene Sheet Using Alkali Metal Carbonates, J. Phys. Chem. C, 116 (2012) 26586-26591. https://doi.org/10.1021/jp3069927
[34] J.C. Meyer, A.K. Geim, M.I. Katsnelson, K.S. Novoselov, T.J. Booth, S. Roth, The structure of suspended graphene sheets, Nature, 446 (2007) 60-63. https://doi.org/10.1038/nature05545
[35] D. Lee, J. Seo, Three-dimensionally networked graphene hydroxide with giant pores and its application in supercapacitors, Sci. Rep., 4 (2014) 7419. https://doi.org/10.1038/srep07419
[36] A.Y. Lee, K. Yang, N.D. Anh, C. Park, S.M. Lee, T.G. Lee, M.S. Jeong, Raman study of D* band in graphene oxide and its correlation with reduction, Appl. Surf. Sci., 536 (2021) 147990. https://doi.org/10.1016/j.apsusc.2020.147990
[37] I. Childres, L.A. Jauregui, W. Park, H. Cao, Y.P. Chen, Raman spectroscopy of graphene and related materials, New developments in photon and materials research, 1 (2013) 1-20.
[38] High Resolution XPS of Organic Polymers: The Scienta ESCA300 Database (Beamson, G.; Briggs, D.), J. Chem. Educ., 70 (1993) A25. https://doi.org/10.1021/ed070pA25.5
[39] M.C. Biesinger, Accessing the robustness of adventitious carbon for charge referencing (correction) purposes in XPS analysis: Insights from a multi-user facility data review, Appl. Surf. Sci., 597 (2022) 153681. https://doi.org/10.1016/j.apsusc.2022.153681
[40] B. Rousseau, H. Estrade-Szwarckopf, X-ray and UV photoelectron spectroscopy study of Na–halogen–graphite intercalation compounds. Comparison between donor- and acceptor-graphite compounds, Solid State Commun., 126 (2003) 583-587. https://doi.org/10.1016/S0038-1098(03)00258-8
[41] J.A. Donadelli, A. Cánneva, G. Erra, A. Calvo, XPS direct analysis on shale rocks: Correlation with kerogen type and maturity, Fuel, 257 (2019) 116004. https://doi.org/10.1016/j.fuel.2019.116004
[42] F. Liang, J.M. Beach, P.K. Rai, W. Guo, R.H. Hauge, M. Pasquali, R.E. Smalley, W.E. Billups, Highly Exfoliated Water-Soluble Single-Walled Carbon Nanotubes, Chem. Mater., 18 (2006) 1520-1524. https://doi.org/10.1021/cm0526967
[43] R. Precht, S. Stolz, E. Mankel, T. Mayer, W. Jaegermann, R. Hausbrand, Investigation of sodium insertion into tetracyanoquinodimethane (TCNQ): results for a TCNQ thin film obtained by a surface science approach, PCCP, 18 (2016) 3056-3064. https://doi.org/10.1039/c5cp06659j
[44] S. Naghdi, H.Y. Song, A. Várez, K.Y. Rhee, S.W. Kim, Engineering the electrical and optical properties of graphene oxide via simultaneous alkali metal doping and thermal annealing, J. MATER. RES. TECHNOL., 9 (2020) 15824-15837. https://doi.org/10.1016/j.jmrt.2020.10.016

[45] D. Tan, W. Zhang, X. Wang, S. Koirala, Y. Miyauchi, K. Matsuda, Polarization-sensitive and broadband germanium sulfide photodetectors with excellent high-temperature performance, Nanoscale, 9 (2017) 12425-12431. https://doi.org/10.1039/C7NR03040A